



# Switching between Stacked Toroids and Helical Supramolecular Polymers in Aqueous Nanotubules

Huaxin Wang and Myongsoo Lee\*

**Although significant advances have been made in supramolecular tubules, reversible polymerization in the tubular walls while maintaining their intact structure remains a great challenge. Here, reversible helical supramolecular polymerization of stacked toroids is reported, while maintaining tubular structures in aqueous solution. At room temperature, the tubules consist of discrete toroid stackings with hydrophobic interior. Upon heating, the tubules based on toroid stackings undergo a reversible helical supramolecular polymerization to transform into helical tubules by interconnecting between spirally open toroids. The helical polymerization arises from a tilting transition of the closed toroids that transform into spirally open toroids driven by the thermal dehydration of a hydrophilic oligoether dendron surrounding the toroid frameworks.**

Tubular structures are ubiquitous in many biological systems such as protein folding and stacked toroids.<sup>[1–5]</sup> Inspired by biological tubules, a great deal of effort has been devoted to design synthetic molecules that are able to self-assemble into folded helical tubules<sup>[6,7]</sup> and nanotubules with stacked toroids,<sup>[8–11]</sup> which is analogous to the protein tubules in nature. The tubules based on helical folding can be constructed by supramolecular approaches. A typical example is provided by folding of linear oligomers with conformationally flexible aromatic skeletons.<sup>[12]</sup> The linear oligomer chains are folded into a helical tubular conformation through reversible noncovalent interactions. The dynamic nature of the helical folding allows environmental changes to influence their functions that are not easily attainable with traditional covalent polymer chains. Another approach to induce hollow tubules is a supramolecular polymerization of stacked toroids. For example, water-soluble, supramolecular toroidal objects with hydrophobic interior

undergo tubular polymerization when they encapsulate a hydrophobic guest within their internal cavities.<sup>[13]</sup> Helically twist stacking of noncovalent macrocycles surrounded by hydrophilic dendrons can give rise to dynamic hollow tubules that undergo reversible helicity switching followed by expansion–contraction motion in response to environmental changes.

Nevertheless, most of the synthetic toroids suffer from a lack of ring opening capability necessary for polymerization, which is in great contrast to natural toroids. Protein toroids in nature are able to helically polymerize to exhibit adaptive functions such as DNA replication,<sup>[14]</sup> microtubule severing,<sup>[15,16]</sup>

and protecting genomic materials.<sup>[17–19]</sup> Thus, the challenge in toroid assembly is how to confer dynamic switching functions with spiral opening for helical polymerization.<sup>[20,21]</sup> We have recently shown that energy input drives supramolecular toroids to initiate helical polymerization through switching into spiral opening.<sup>[22]</sup> As a result of the exposure of the hydrophobic cross sections of the open form to hydrophilic environment, the toroidal objects autonomously undergo helical polymerization through end-to-end connection. However, the reversible helical polymerization of the stacked toroids while maintaining a tubular structure remains elusive.

Here, we report the formation of tubular structures consisting of discrete toroid stackings by self-assembly of an aromatic macrocycle amphiphile with a hydrophilic oligoether dendron in aqueous solution. At room temperature, the amphiphilic molecule self-assembles into toroidal structures that stack on top of each other to form nanotubules with hydrophobic interior. Upon heating, the tubules based on discrete toroid stackings undergo reversible helical supramolecular polymerization to transform into helical tubules with induced Cotton effect. The helical polymerization originates from interconnection of spirally open toroids formed through a tilting transition of the closed toroids driven by the thermal dehydration of a hydrophilic oligoether dendron surrounding the toroid frameworks (**Figure 1**). We envisioned that, when a planar aromatic macrocycle is grafted by a hydrophilic dendron at one end, the wedge-shaped molecular geometry with a fixed aromatic conformation would generate curved tubules based on toroid stacks with hydrophobic interior, different from the stable toroidal structure of conformationally flexible aromatic dimer.<sup>[22]</sup> In this context, we synthesized a naphthalene-based,

H. Wang, Prof. M. Lee  
State Key Lab of Supramolecular Structure and Materials  
College of Chemistry  
Jilin University  
Changchun 130012, China  
Prof. M. Lee  
Department of Chemistry  
Fudan University  
Shanghai 200438, China  
E-mail: mslee@fudan.edu.cn

The ORCID identification number(s) for the author(s) of this article can be found under <https://doi.org/10.1002/marc.202000138>.

DOI: 10.1002/marc.202000138

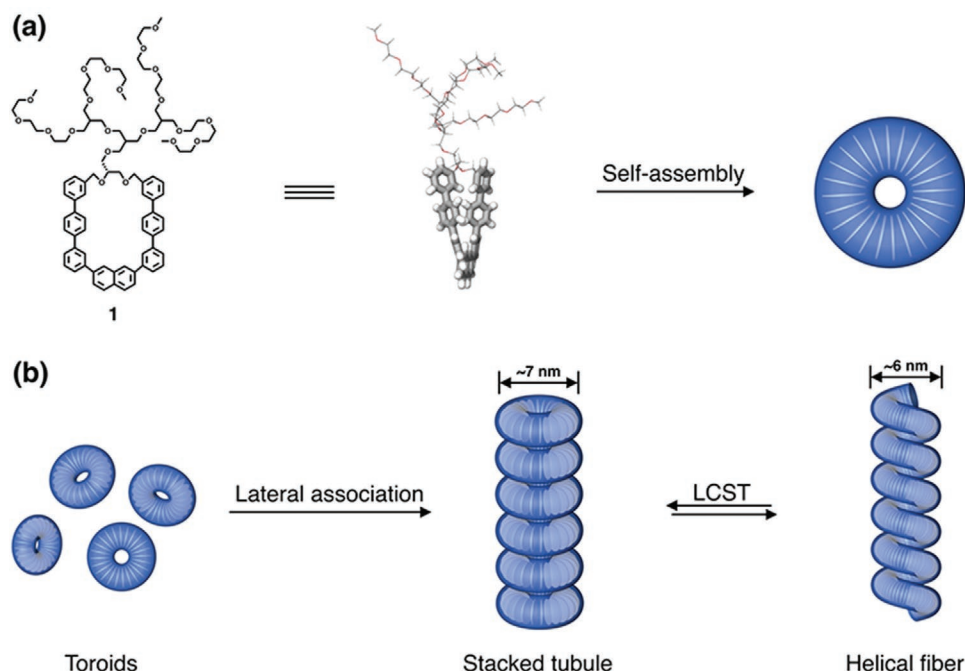


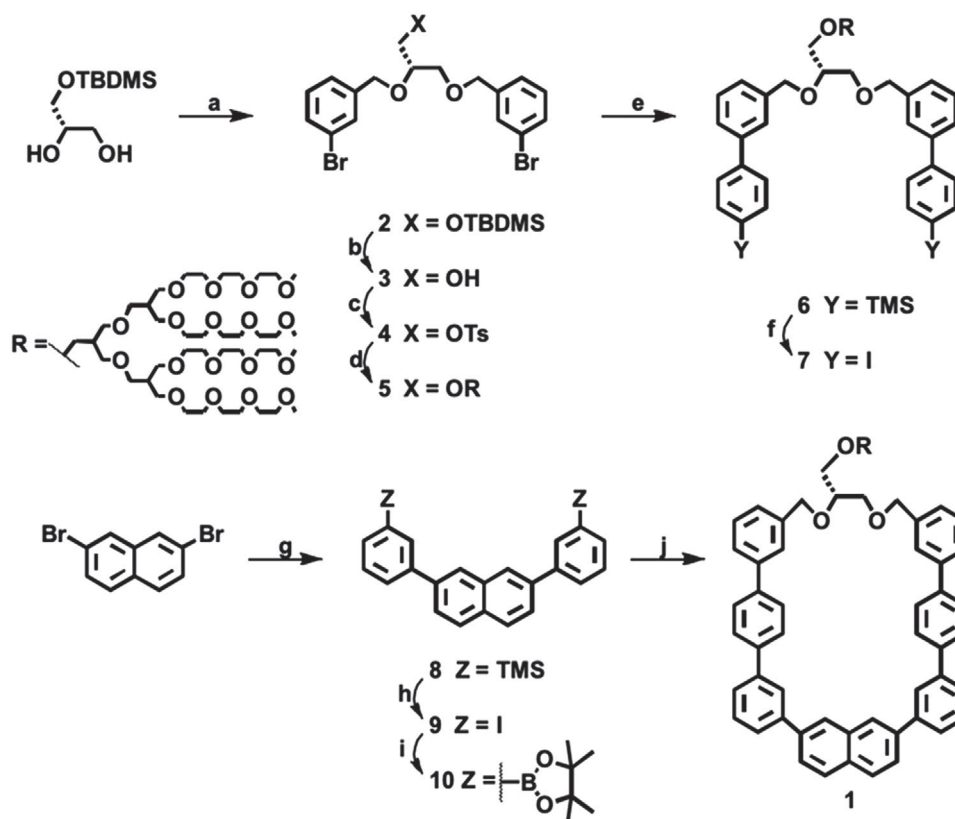
**Figure 1.** a) Molecular structure of amphiphile **1**. b) Schematic representation of reversible helical polymerization of tubule stacked by toroid **1** with rapid response to heating–cooling treatments.

planar aromatic macrocycle with a hydrophilic chiral dendron at the one end of the aromatic segment.

The molecule that undergoes a helical polymerization in tubular structures consists of an aromatic macrocycle grafted by a hydrophilic oligoether dendron, which was synthesized in a stepwise fashion according to the procedures described in the experimental section (Scheme 1). Previously, we reported that a dimeric aromatic macrocycle amphiphile with bulky hydrophilic dendrimers self-assembles into discrete toroidal structures.<sup>[22]</sup> Considering such results, we envisioned that a decreased relative volume fraction of the hydrophilic chain to the aromatic segment drives discrete toroids to stack on top of each other, forming hollow tubules. Indeed, transmission electron microscopy (TEM) of molecule **1** showed the formation of hollow tubules with a uniform external diameter of 7 nm (Figure 2a). Close examinations of the image revealed a dark interior separated by a white periphery, demonstrating that the 1D fiber-like objects are based on hollow interior (Figure 2a, inset).<sup>[23]</sup> The formation of the tubular structures was further confirmed using cryogenic transmission electron microscopy (cryo-TEM) with the vitrified solution, which provides an additional evidence that the aggregates exist as tubular structures in bulk solution (Figure 2b). Atomic force microscopy (AFM) image showed closely packed, tubular aggregates with a diameter of  $\approx 7$  nm (Figure 2c), consistent with the result observed by TEM. Notably, the surfaces of the tubules consist of lateral stripes with an average spacing of  $\approx 3$  nm along the fiber axis, implying that the tubular objects consist of stacked toroids. To confirm the primary structure of the tubules, we examined the diluted solution of **1** using TEM (Figure 2d). The image obtained from diluted conditions revealed discrete toroidal objects with a

diameter of  $\approx 7$  nm, demonstrating that the tubules are based on stacked toroids. Molecular dynamic simulations showed that the toroidal structure is composed of curved assembly of 30 molecules of **1** with aromatic interior surrounded by hydrophilic chains (Figure 2e). To confirm the hydrophobic interior, we performed encapsulation experiments with hydrophobic  $C_{60}$  guest. Upon addition of  $C_{60}$  into the tubule solution at room temperature, the fluorescence emission associated with the tubular structure remarkably decreased up to 0.06 eq relative to **1**. of the guest and then leveled off (Figure 2f), indicating that the internal surface of the tubular pore is hydrophobic.<sup>[24]</sup> Considering that the toroid consists of 30 molecules of **1** (Figure 2e), this result indicates that one toroid includes a maximum amount of approximately 1.8  $C_{60}$  molecules per toroid cavity.

Oligoether chains are well known to undergo thermal dehydration on heating to collapse into a globular shape that influences on aromatic packings.<sup>[25]</sup> Indeed, the solution on heating to 60 °C of **1** appears a strong circular dichroism (CD) signals together with red-shifted UV absorption (Figure 3a,b), indicating that the randomly overlapped aromatic packings in the toroidal frameworks are slipped in a preferred direction against one another due to an increased cross-sectional area of the globular dendrons and strengthened hydrophobic interactions. Notably, even after thermal dehydration of the oligoether chains, the tubular structures remained unchanged except slight decrement in their external diameter to  $\approx 6$  nm (Figure 3c,d), demonstrating that the thermal dehydration of the oligoether chains drives the tubules to undergo a molecular rearrangement within their walls from randomly overlapped to slipped chiral packings. Indeed, AFM investigations revealed a left-handed helical structure with an average pitch distance of 3.5 nm (Figure 3e),



Scheme 1. Synthetic method of amphiphile 1.

which implies that molecular slipping on heating leads to a helical transition in the tubules based on stacked toroids.

To gain insight into the helicity induction in the tubular structure, we performed TEM experiments with a diluted solution of 1 at 60 °C. The image showed short, curled fibrils with a diameter of  $\approx 3$  nm rather than discrete toroidal objects (Figure 3f), indicating that the tubules formed at higher temperatures are based on folded helical chains rather than stacked toroidal objects. In the solution at room temperature, the aromatic macrocycles with overlapped packings are approximately perpendicular to the plane of the toroid to maximize aromatic interactions. Upon heating, however, the dehydrated oligoether dendrons would make the overlapped packings of the macrocycles to be unstable due to steric hindrance between the globular-shaped dendrons with a greater cross-section.<sup>[22,25,26]</sup> To relieve the steric hindrance at the interface, the macrocycle planes would be tilted through slipping with respect to each other to allow a larger interfacial area, thus breaking closed toroids to be spirally open (Figure 3g). As a result of the exposure of the hydrophobic cross sections of the open ends of the toroids to hydrophilic environment, the spirally open toroids are interconnected with each other through end-to-end aromatic interactions to form helical tubules (Figure 1b). The helical structuring, together with all the spectral changes, is fully reversible on cooling and subsequent heating cycles (Figure 3h).

In summary, our results demonstrate that the tubular structures based on stacked toroids with hydrophobic interior can undergo reversible supramolecular polymerization to form

helical tubules upon heating. This structural transformation of the tubules is based on helical polymerization of spirally open toroids driven by a tilting transition of the stacked toroids. Considering that most of the supramolecular toroids stacked in a tubule are insensitive to polymerization, the notable feature of our tubules is their ability to perform helical polymerization of stacked toroids through reversible switching between closed and spirally open toroids. Such a unique tubular wall will offer an opportunity to explore temperature-responsive nanoreactors for chemical transformations due to different spatial confinements, which is undergoing in our lab.

## Experimental Section

**Methods:** All reactions were performed in oven-dried glassware under dry argon atmosphere. Toluene and THF were dried by distillation from sodium-benzophenone immediately prior to use. Dichloromethane (DCM) and pyridine were dried by distillation from  $\text{CaH}_2$ . Distilled water was polished by ion exchange and filtration. Other solvents and organic reagents were purchased from commercial vendors and used without further purification unless otherwise mentioned. The reactions were monitored by thin-layer chromatography (TLC; Merck, silica gel 60 F254 0.25 mm) with visualization under UV light (254 nm) or treating iodine, phosphomolybdic acid. The products were purified by flash column chromatography on silica gel (230–400 mesh). Recycling preparative high-pressure chromatography (HPLC) was performed for further purification of the final desired molecules by using Prominence LC-20AP (SHIMADZU) and YMC C8 reverse phase column (250  $\times$  4.6 mm ID, S 5  $\mu\text{m}$ , 12 nm and 250  $\times$  20.0 mm ID, S

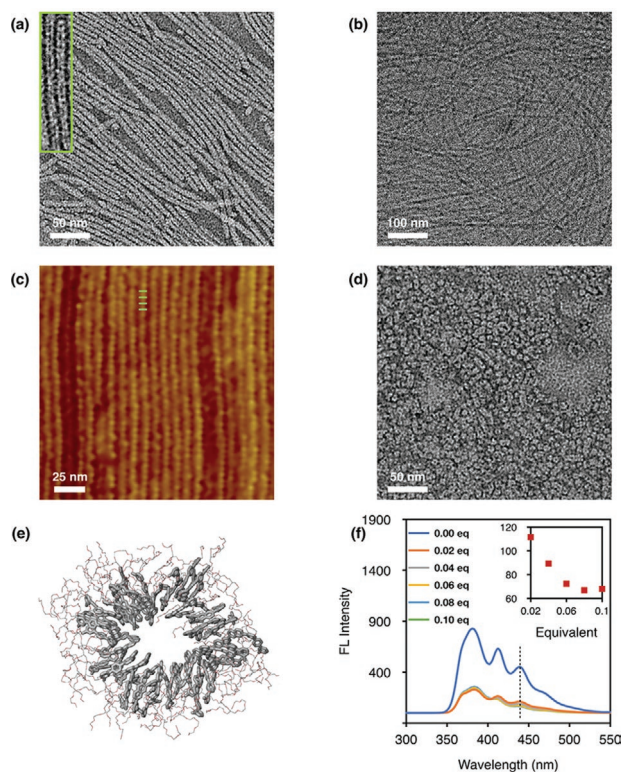


**Figure 2.** a) Negatively stained TEM images of **1** ( $64.5 \times 10^{-6}$  M) in  $\text{H}_2\text{O}$ . b) Cryo-TEM image of **1** ( $64.5 \times 10^{-6}$  M) in  $\text{H}_2\text{O}$  below LCST ( $25^\circ\text{C}$ ). c) AFM image of **1** ( $64.5 \times 10^{-6}$  M) in  $\text{H}_2\text{O}$  below LCST ( $25^\circ\text{C}$ ) on mica. d) Negatively stained TEM images of **1** in diluted condition ( $12.9 \times 10^{-6}$  M) in  $\text{H}_2\text{O}$ . e) Molecular dynamic simulation of toroid consisting of 30 molecules, resulting in hydrophobic interior with a diameter of 1.2 nm. f) Fluorescence spectra of **1** with different equivalent  $\text{C}_{60}$  in  $\text{H}_2\text{O}$  (inset: fluorescence intensity variation of **1** with different equivalent of  $\text{C}_{60}$  at 436 nm). Excitation wavelength: 280 nm.

5  $\mu\text{m}$ , 12 nm).  $^1\text{H}$ -NMR and  $^{13}\text{C}$ -NMR spectra were recorded on Bruker AVANCE III 500. All compounds were subjected to  $^1\text{H}$  NMR analysis to confirm  $\geq 98\%$  sample purity. Chemical shifts were reported in ppm relative to the residual solvent peak ( $\text{CDCl}_3$ :  $^1\text{H}$ , 7.26;  $^{13}\text{C}$ , 77.23) or tetramethylsilane (TMS) peak. Multiplicity was indicated as follows: s (singlet), d (doublet), t (triplet), q (quartet), m (multiplet), dd (doublet of doublets), dt (doublet of triplets), td (triplet of doublets). Coupling constants are reported in Hertz (Hz). Matrix-assisted laser desorption/ionization time of flight mass spectrometry (MALDI-TOF-MS) was performed on a Bruker Microflex LRF20 using trans-2-[3-(4-tert-butylphenyl)-2-methyl-2-propenyli-dene]malononitrile (DCTB) as a matrix. UV-vis spectra were obtained from a Hitachi U-2900 Spectrophotometer. Fluorescence spectra were obtained from a Hitachi F7000 Fluorescence Spectrophotometer. Dynamic light scattering (DLS) measurement was performed using an ALV/CGS-3. CD spectra were obtained using Jasco J-810 spectropolarimeter. Molecular modeling and calculations were performed by Desmond module within the molecular modeling suite Maestro from Schrödinger Suites (Schrödinger K.K.).

**Methods—TEM Experiments:** To investigate the self-assembled structures in aqueous solution, a drop of each sample solution was placed on a carbon-coated copper grid (Carbon Type B (15–25 nm) on 200 mesh, with Formvar; Ted Pella, Inc.) and the solution was allowed to evaporate under ambient conditions. These samples were stained by depositing a drop of uranyl acetate aqueous solution (0.4–1.0 wt%) onto the surface of the sample-loaded grid. The dried specimen was observed

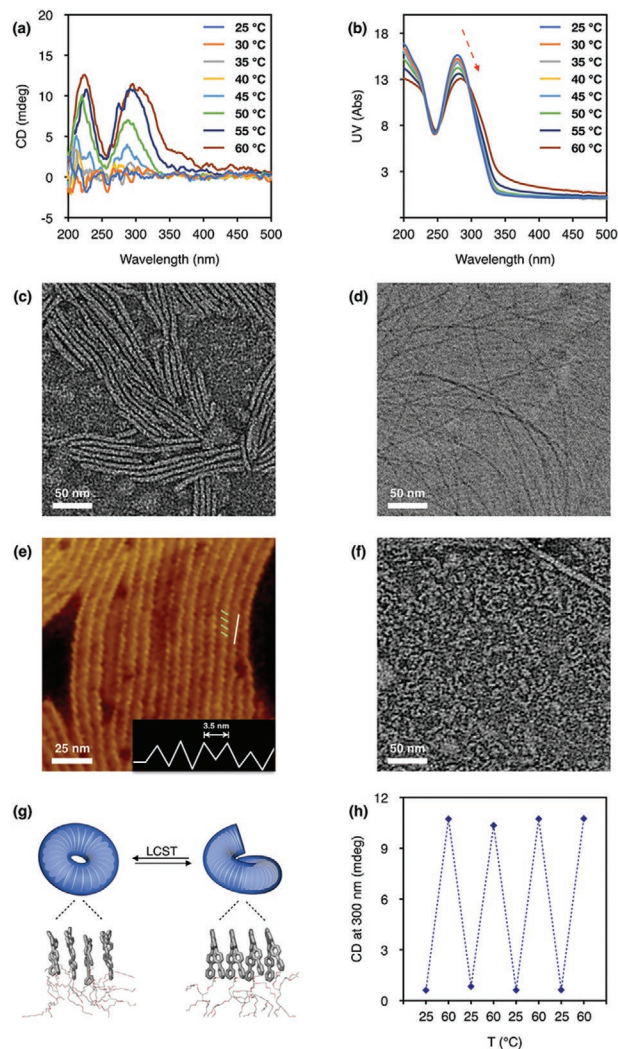


**Figure 3.** a) Temperature-dependent CD spectra of **1** ( $193.5 \times 10^{-6}$  M) in  $\text{H}_2\text{O}$ . b) Temperature-dependent UV-vis spectra of **1** ( $193.5 \times 10^{-6}$  M) in  $\text{H}_2\text{O}$ . c) Negatively stained TEM images of **1** ( $193.5 \times 10^{-6}$  M) in  $\text{H}_2\text{O}$  above LCST ( $60^\circ\text{C}$ ). d) Cryo-TEM image of **1** ( $193.5 \times 10^{-6}$  M) in  $\text{H}_2\text{O}$  above LCST ( $60^\circ\text{C}$ ). e) AFM image of **1** in  $\text{H}_2\text{O}$  above LCST ( $60^\circ\text{C}$ ) on mica. f) Negatively stained TEM images of **1** in diluted condition ( $12.9 \times 10^{-6}$  M) in  $\text{H}_2\text{O}$  at  $60^\circ\text{C}$ . g) Schematic representation of temperature-driven reversible toroid opening and close. h) CD intensity (300 nm) variation of **1** ( $193.5 \times 10^{-6}$  M) in  $\text{H}_2\text{O}$  with repeated heating/cooling cycles.

by a JEOL-JEM HR2100 operated at 120 kV. The cryo-TEM experiments were performed with a thin film of aqueous solution of amphiphiles (3  $\mu\text{L}$ ) transferred to a lacey supported grid. The thin aqueous films were prepared under controlled temperature and humidity conditions (97–99%) within a custom-built environmental chamber in order to prevent evaporation of water from sample solution. The excess liquid was blotted with filter paper for 2–3 s, and the thin aqueous films were rapidly vitrified by plunging them into liquid ethane (cooled by liquid nitrogen) at its freezing point. The grid was transferred, on a Gatan 626 cryoholder, using a cryotransfer device and transferred to the JEOL-JEM HR2100 TEM. Direct imaging was carried out at a temperature of approximately  $-175^\circ\text{C}$  and with a 120 kV accelerating voltage, using the images acquired with a Dual vision 300 W and SC 1000 CCD camera (Gatan, Inc.; Warrendale, PA). The data were analyzed using Digital Micrograph software.

**Methods—AFM Experiments:** The sample films on mica surface were prepared from evaporation of sample solutions. The measurements were conducted on a MultiMode 8 AFM with NanoScope V controller, NanoScope software and NanoScope Analysis software (Bruker AXS Corporation, Santa Barbara, CA, USA) in air at ambient temperature ( $\approx 25$  °C) in the scanasyt in air mode.

**Method—Sampling Method:** All sample solutions were prepared by evaporation of a  $\text{CHCl}_3$  mixture of **1** ( $64.5 \times 10^{-6}$  M), then water was added to the dry film and the solution was sonicated for 30 min in ice bath. The solution was then stored for 8 h. As for the sample solution with the addition of  $\text{C}_{60}$ ,  $\text{C}_{60}$  film was first prepared and the aqueous solution followed by the method above was added to the dry film and the solution was treated with sonication for 5 min in ice bath. The solution was stand at least 8 h at 4 °C.

**Methods—DLS Experiments:** The dynamic light scattering experiments were performed by ALV/CFS-3 using He–Ne laser operating at 632.8 nm. The scattering was kept at 90° during the whole experiment at 25 °C. The hydrodynamic diameter was determined from autocorrelation functions by the time interval method of photon correlation and the CONTIN method using the software provided by the manufacturer. To avoid the influence of dust, all solutions were filtered through a 0.45  $\mu\text{m}$  membrane filter.

**Methods—Molecular Dynamic Simulation:** The self-assembled toroid was simulated with MD using the Desmond module within Maestro from Schrödinger Suites with the following parameters-force field: OPLS3; solvent: SPC; simulation temperature: 300.0 K; pressure: 1.01325 bar; simulation time: 10 ns.

**Synthetic Method—Reagents and Conditions:** (a) 1-Bromo-3-(bromomethyl)benzene, NaH, THF, 70 °C, overnight, yield, 53%; (b) tetrabutylammonium fluoride, AcOH, THF, rt, overnight, yield, 95%; (c) TsCl, pyridine, rt, overnight, yield, 52%; (d) ROH, NaH, THF, 70 °C, overnight, yield, 32%; (e) 4-trimethylsilylphenylboronic acid,  $\text{Pd}(\text{PPh}_3)_4$ , 2 M  $\text{Na}_2\text{CO}_3$  (aq), ethanol, toluene, reflux, overnight, yield, 63%; (f) ICl, DCM, 0 °C, 4 h, yield, 83%; (g) 3-trimethylsilylphenylboronic acid,  $\text{Pd}(\text{PPh}_3)_4$ , 2 M  $\text{Na}_2\text{CO}_3$  (aq), ethanol, toluene, reflux, overnight, yield, 46%; (h) ICl, DCM, 0 °C, 2 h, yield, 95%; (i) bis(pinacolato)diboron,  $\text{Pd}(\text{dppf})\text{Cl}_2$ , KOAc, DMF, 100 °C, overnight, yield, 62%; (j) compound **7**,  $\text{Pd}(\text{PPh}_3)_4$ , 2 M  $\text{Na}_2\text{CO}_3$  (aq), ethanol, toluene, reflux, overnight, yield, 18%.

**Compound 2.** (S)-3-((*tert*-Butyldimethylsilyloxy)propane-1,2-diol (473.8 mg, 2.30 mmol) was dissolved in distilled THF (23.0 mL), and NaH (60%) (459.7 mg, 11.49 mmol) was added slowly in ice bath. After stirring for 15 min, 1-bromo-3-(bromomethyl)benzene (1253.5 mg, 5.06 mmol) was added and the reaction was heated to 70 °C and stirring overnight under Ar atmosphere. After completion of the reaction as monitored by TLC, the reaction mixture was cooled down to room temperature. The resulting mixture was condensed under reduced pressure, and dissolve in ethyl acetate. The organic layer was washed with brine and dried over  $\text{MgSO}_4$  (s). The organic phase was filtered with Celite and the filtrate was condensed in a rotary evaporator. The crude product was purified by flash silica gel chromatography (eluent condition: DCM:hexane = 1:2, v/v) to provide 53% yield as colorless oil.

$^1\text{H}$  NMR (500 MHz, chloroform-*d*)  $\delta$  7.50 (dd,  $J = 17.4, 1.9$  Hz, 2H), 7.40 (tt,  $J = 7.4, 1.6$  Hz, 2H), 7.30–7.23 (m, 4H), 7.20 (q,  $J = 7.5$  Hz, 2H), 4.67 (s, 2H), 4.51 (s, 2H), 3.71 (d,  $J = 6.1$  Hz, 2H), 3.68–3.60 (m, 2H), 3.58–3.53 (m, 1H), 0.89 (s, 9H), 0.05 (s, 6H).  $^{13}\text{C}$  NMR (126 MHz,  $\text{CDCl}_3$ )  $\delta$  141.19, 140.70, 130.61, 130.52, 130.49, 129.94, 126.02, 125.98, 122.52, 122.47, 79.24, 72.56, 71.50, 70.51, 62.98, 25.89, 18.28, –5.50.

**Compound 3.** Compound **2** (1003.2 mg, 1.85 mmol) was dissolved in dry THF (7.4 mL), tetrabutylammonium fluoride (1.0 M in THF solution) (3.70 mL, 3.70 mmol) and AcOH (133.4 mg, 2.22 mmol) were then added in the flask and stirring at room temperature overnight under Ar atmosphere. After completion of the reaction as monitored by TLC, the resulting mixture was condensed under reduced pressure, and dissolved in ethyl acetate. The organic layer was washed with brine and dried over  $\text{MgSO}_4$  (s). The organic layer was filtered and condensed under reduced vacuum. The crude product was purified by flash silica gel column chromatography (ethyl acetate:hexane = 1:3, v/v) to provide 95% yield as colorless oil.

$^1\text{H}$  NMR (500 MHz, chloroform-*d*)  $\delta$  7.48 (d,  $J = 16.9$  Hz, 2H), 7.42–7.36 (m, 2H), 7.27–7.15 (m, 4H), 4.67–4.55 (m, 2H), 4.48 (s, 2H), 3.77–3.56 (m, 5H), 2.43 (bs, 1H).  $^{13}\text{C}$  NMR (126 MHz,  $\text{CDCl}_3$ )  $\delta$  140.60, 140.28, 130.83, 130.62, 130.52, 130.05, 126.12, 126.03, 122.59, 78.45, 77.29, 77.03, 76.78, 72.70, 71.38, 70.44, 62.71.

**Compound 4.** Compound **3** (680.9 mg, 1.58 mmol) was dissolved in dry pyridine (2.6 mL) and TsCl (332.1 mg, 1.75 mmol) was added and the reaction was stirred at room temperature overnight under Ar atmosphere. After completion of the reaction as monitored by TLC, the resulting mixture was quenched with HCl (2 M). The mixture was extracted with DCM and the organic layer was combined, washed with brine and dried over  $\text{MgSO}_4$  (s). Then the organic phase was filtered and condensed under reduced vacuum. The crude product was purified by flash silica gel column chromatography (ethyl acetate:hexane = 1:5, v/v) to provide 52% yield as white solid.

$^1\text{H}$  NMR (400 MHz, chloroform-*d*)  $\delta$  7.81 (d,  $J = 8.3$  Hz, 2H), 7.46 (qd,  $J = 4.0, 3.4, 2.2$  Hz, 4H), 7.37–7.33 (m, 2H), 7.26–7.21 (m, 4H), 4.58 (s, 2H), 4.47 (s, 2H), 4.25 (dd,  $J = 10.5, 4.2$  Hz, 1H), 4.15 (dd,  $J = 10.5, 5.8$  Hz, 1H), 3.83 (qd,  $J = 5.3, 4.2$  Hz, 1H), 3.57 (d,  $J = 5.1$  Hz, 2H), 2.47 (s, 3H).  $^{13}\text{C}$  NMR (126 MHz,  $\text{CDCl}_3$ )  $\delta$  144.96, 140.13, 140.07, 132.69, 130.83, 130.51, 130.43, 130.03, 129.97, 129.89, 127.95, 126.08, 125.98, 122.55, 122.50, 77.29, 77.03, 76.78, 75.84, 72.61, 71.54, 69.22, 69.08, 53.44, 21.68, 0.01.

**Compound 5.** ROH (1028.8 mg, 1.19 mmol) was dissolved in distilled THF (4.0 mL), and NaH (60%) (118.7 mg, 2.97 mmol) was added slowly in ice bath. After stirring for 15 min, compound **4** (760.0 mg, 1.31 mmol) was added and the reaction was heated to 70 °C and stirring overnight under Ar atmosphere. After completion of the reaction as monitored by TLC, the reaction mixture was cooled down to room temperature. The resulting mixture was condensed under reduced pressure, and dissolve in ethyl acetate. The organic layer was washed with brine and dried over  $\text{MgSO}_4$  (s). The organic phase was filtered with Celite and the filtrate was condensed in a rotary evaporator. The crude product was purified by flash silica gel chromatography (eluent condition: methanol:ethyl acetate = 1:10, v/v) to provide 32% yield as colorless oil.

$^1\text{H}$  NMR (500 MHz, chloroform-*d*)  $\delta$  7.52 (t,  $J = 1.7$  Hz, 1H), 7.48 (d,  $J = 1.7$  Hz, 1H), 7.43–7.38 (m, 2H), 7.30–7.18 (m, 4H), 4.66 (d,  $J = 4.0$  Hz, 2H), 4.51 (s, 2H), 3.67–3.36 (m, 83H), 2.15 (m, 3H).  $^{13}\text{C}$  NMR (126 MHz,  $\text{CDCl}_3$ )  $\delta$  141.13, 140.64, 130.62, 130.49, 130.46, 130.40, 129.99, 129.89, 126.01, 125.96, 122.48, 122.42, 77.51, 77.35, 77.10, 76.84, 72.51, 71.91, 71.38, 71.29, 70.79, 70.60, 70.56, 70.50, 70.45, 69.95, 69.68, 69.46, 59.00, 40.25, 40.13. MALDI-TOF mass:  $m/z$  calcd. for  $\text{C}_{57}\text{H}_{98}\text{Br}_2\text{NaO}_{21}$  [ $\text{M} + \text{Ma}$ ] $^+$ , 1302.188; found, 1301.300.

**Compound 6.** Compound **5** (488.7 mg, 0.38 mmol), 4-trimethylsilylphenylboronic acid (163.5 mg, 0.84 mmol),  $\text{Pd}(\text{PPh}_3)_4$  (4.4 mg, 0.004 mmol) were refluxed in mixture of 2 M aqueous  $\text{Na}_2\text{CO}_3$  (1.0 mL), ethanol (1.9 mL) and toluene (3.8 mL) for overnight under Ar atmosphere. After completion of the reaction as monitored by TLC, the reaction mixture was cooled down to room temperature. The resulting mixture was condensed under reduced pressure, and dissolve in ethyl acetate. The organic layer was washed with brine and dried over  $\text{MgSO}_4$  (s). The organic phase was filtered with Celite and the filtrate was condensed in a rotary evaporator. The crude product was purified by flash silica gel chromatography (eluent condition: methanol:ethyl acetate = 1:10, v/v) to provide 63% yield as pale yellow liquid.

$^1\text{H}$  NMR (500 MHz, chloroform-*d*)  $\delta$  7.56 (d,  $J = 2.8$  Hz, 10H), 7.50 (ddt,  $J = 8.8, 6.8, 1.7$  Hz, 2H), 7.40–7.31 (m, 4H), 4.77 (d,  $J = 2.2$  Hz, 2H), 4.62 (s, 2H), 3.86–3.80 (m, 1H), 3.70–3.51 (m, 50H), 3.46 (d,  $J = 5.9$  Hz, 12H), 3.42–3.34 (m, 20H), 2.14 (dp,  $J = 12.2, 6.0$  Hz, 3H), 0.29 (s, 18H).  $^{13}\text{C}$  NMR (126 MHz,  $\text{CDCl}_3$ )  $\delta$  141.45, 141.37, 141.22, 141.14, 139.31, 139.25, 139.17, 138.89, 133.78, 128.84, 128.77, 126.72, 126.55, 126.48, 126.40, 126.37, 126.30, 77.41, 77.30, 77.05, 76.80, 73.44, 72.31, 71.94, 71.47, 70.88, 70.63, 70.59, 70.53, 70.48, 69.98, 69.71, 69.50, 59.03, 40.30, 40.17, –1.06. MALDI-TOF mass:  $m/z$  calcd. for  $\text{C}_{75}\text{H}_{124}\text{NaO}_{21}\text{Si}_2$  [ $\text{M} + \text{Ma}$ ] $^+$ , 1440.956; found, 1442.300.

**Compound 7.** Compound **6** (467.1 mg, 0.33 mmol) was dissolved in anhydrous DCM (3.3 mL). ICl (1.0 M in DCM solution) (0.36 mL, 0.36 mmol) was added dropwise to the reaction solution in ice bath.

The mixture was stirred in ice bath for 2 h under Ar atmosphere. After completion of the reaction as monitored by MALDI-TOF-MS, the reaction was quenched with Na<sub>2</sub>S<sub>2</sub>O<sub>3</sub> saturated aqueous solution. The organic layer was washed with brine and dried over MgSO<sub>4</sub> (s). The organic phase was filtered with Celite and the filtrate was condensed in a rotary evaporator. The crude product was purified by flash silica gel chromatography (eluent condition: methanol:ethyl acetate = 1:10, v/v). Finally, the purified precursor was further purified by prep-HPLC (C8 column ACN:H<sub>2</sub>O = 80:20 v/v) to provide 83% yield as white waxy solid.

<sup>1</sup>H NMR (500 MHz, chloroform-*d*) δ 7.74–7.69 (m, 4H), 7.53 (d, *J* = 1.6 Hz, 1H), 7.51 (d, *J* = 1.7 Hz, 1H), 7.44 (ddt, *J* = 10.6, 7.3, 1.7 Hz, 2H), 7.40–7.27 (m, 8H), 4.80–4.73 (m, 2H), 4.61 (s, 2H), 3.85–3.80 (m, 1H), 3.68–3.52 (m, 54H), 3.46 (dd, *J* = 6.0, 2.5 Hz, 10H), 3.37 (s, 20H), 2.13 (dp, *J* = 17.4, 6.0 Hz, 3H). <sup>13</sup>C NMR (126 MHz, CDCl<sub>3</sub>) δ 140.56, 140.47, 140.12, 140.04, 139.51, 139.08, 137.82, 137.79, 128.98, 128.90, 126.98, 126.84, 126.09, 126.07, 126.02, 125.94, 93.10, 93.03, 77.46, 77.29, 77.03, 76.78, 73.28, 72.16, 71.94, 71.40, 70.94, 70.64, 70.59, 70.54, 70.48, 69.99, 69.71, 69.50, 59.04, 40.28, 40.16. MALDI-TOF mass: *m/z* calcd. for C<sub>69</sub>H<sub>106</sub>NaO<sub>21</sub> [M + Na]<sup>+</sup>, 1548.385; found, 1548.597.

**Compound 8.** 2,7-Dibromonaphthalene (500.0 mg, 1.75 mmol), 3-trimethylsilylphenylboronic acid (746.7 mg, 3.85 mmol), Pd(PPh<sub>3</sub>)<sub>4</sub> (20.2 mg, 0.02 mmol) were refluxed in mixture of 2 M aqueous Na<sub>2</sub>CO<sub>3</sub> (4.4 mL), ethanol (8.8 mL) and toluene (17.5 mL) for overnight under Ar atmosphere. After completion of the reaction as monitored by TLC, the reaction mixture was cooled down to room temperature. The resulting mixture was condensed under reduced pressure, and dissolve in ethyl acetate. The organic layer was washed with brine and dried over MgSO<sub>4</sub> (s). The organic phase was filtered with Celite and the filtrate was condensed in a rotary evaporator. The crude product was purified by flash silica gel chromatography (eluent condition: ethyl acetate:hexane = 1:20, v/v) to provide 46% yield as white waxy solid.

<sup>1</sup>H NMR (500 MHz, chloroform-*d*) δ 8.11 (d, *J* = 1.7 Hz, 2H), 7.95 (d, *J* = 8.4 Hz, 2H), 7.87 (t, *J* = 1.5 Hz, 2H), 7.75 (dd, *J* = 8.5, 1.7 Hz, 2H), 7.72 (dt, *J* = 7.6, 1.7 Hz, 2H), 7.56 (dt, *J* = 7.3, 1.3 Hz, 2H), 7.49 (t, *J* = 7.5 Hz, 2H), 0.35 (s, 18H). <sup>13</sup>C NMR (126 MHz, CDCl<sub>3</sub>) δ 141.21, 140.42, 139.42, 133.97, 132.43, 132.35, 131.73, 128.25, 128.16, 128.04, 126.15, 125.87, –1.01.

**Compound 9.** Compound 8 (108.0 mg, 0.25 mmol) was dissolved in anhydrous DCM (2.5 mL). ICl (1.0 M in DCM solution) (0.61 mL, 0.61 mmol) was added dropwise to the reaction solution in ice bath. The mixture was stirred in ice bath for 2 h under Ar atmosphere. After completion of the reaction as monitored by TLC, the reaction was quenched with Na<sub>2</sub>S<sub>2</sub>O<sub>3</sub> saturated aqueous solution. The organic layer was washed with brine and dried over MgSO<sub>4</sub> (s). The organic phase was filtered with Celite and the filtrate was condensed in a rotary evaporator. The crude product was purified by flash silica gel chromatography (eluent condition: ethyl acetate:hexane = 1:20, v/v) to provide 95% yield as white solid.

<sup>1</sup>H NMR (500 MHz, chloroform-*d*) δ 8.09 (t, *J* = 1.7 Hz, 2H), 8.08–8.05 (m, 2H), 7.94 (d, *J* = 8.5 Hz, 2H), 7.74–7.68 (m, 6H), 7.23 (t, *J* = 7.8 Hz, 2H). <sup>13</sup>C NMR (126 MHz, CDCl<sub>3</sub>) δ 143.17, 137.55, 136.38, 133.72, 132.16, 130.54, 128.39, 126.63, 126.32, 125.63, 94.94.

**Compound 10.** Compound 9 (146.0 mg, 0.27 mmol) and bis(pinacolato)diboron (153.1 mg, 0.60 mmol) were dissolved in degassed DMF (2.7 mL), then potassium acetate (134.5 mg, 1.37 mmol) and Pd(dppf)Cl<sub>2</sub> (11.2 mg, 0.01 mmol) were added into the solution. The mixture was heated to 100 °C and stirred overnight under Ar atmosphere. After completion of the reaction as monitored by TLC. The resulting mixture was condensed under reduced pressure, and dissolve in ethyl acetate. The organic layer was washed with brine and dried over MgSO<sub>4</sub> (s). The organic phase was filtered with Celite and the filtrate was condensed in a rotary evaporator. The crude product was purified by flash silica gel chromatography (eluent condition: ethyl acetate:hexane = 1:3, v/v) to provide 62% yield as white solid.

<sup>1</sup>H NMR (500 MHz, chloroform-*d*) δ 8.23 (s, 2H), 8.17 (s, 2H), 7.95 (d, *J* = 8.5 Hz, 2H), 7.90–7.83 (m, 4H), 7.82 (dd, *J* = 8.5, 1.8 Hz, 2H), 7.53 (t, *J* = 7.5 Hz, 2H), 1.41 (s, 24H). <sup>13</sup>C NMR (126 MHz, CDCl<sub>3</sub>) δ 140.38, 138.82, 133.95, 133.80, 133.72, 131.77, 130.25, 128.30, 128.03, 126.18, 125.75, 83.92, 24.93.

**Compound 1.** Compound 7 (100.0 mg, 0.066 mmol), compound 10 (34.9 mg, 0.066 mmol), Pd(PPh<sub>3</sub>)<sub>4</sub> (0.76 mg, 0.00066 mmol) were refluxed in mixture of 2 M aqueous Na<sub>2</sub>CO<sub>3</sub> (1.6 mL), ethanol (3.2 mL) and toluene (6.4 mL) for overnight under Ar atmosphere. After completion of the reaction as monitored by TLC, the reaction mixture was cooled down to room temperature. The resulting mixture was condensed under reduced pressure, and dissolve in ethyl acetate. The organic layer was washed with brine and dried over MgSO<sub>4</sub> (s). The organic phase was filtered with Celite and the filtrate was condensed in a rotary evaporator. The crude product was purified by flash silica gel chromatography (eluent condition: methanol:ethyl acetate = 1:10 v/v). Finally, the purified product was further purified by prep-HPLC (C8 column ACN:H<sub>2</sub>O = 90:10 v/v) to provide 18% yield as white solid.

<sup>1</sup>H NMR (500 MHz, chloroform-*d*) δ 8.32 (t, *J* = 2.5 Hz, 2H), 8.14 (q, *J* = 2.0 Hz, 2H), 7.98 (d, *J* = 8.5 Hz, 2H), 7.89 (dt, *J* = 8.4, 2.3 Hz, 2H), 7.81 (dtd, *J* = 15.8, 8.3, 5.3 Hz, 10H), 7.73 (s, 2H), 7.69 (ddt, *J* = 7.7, 2.0, 1.1 Hz, 2H), 7.61 (qd, *J* = 7.8, 1.3 Hz, 4H), 7.45 (td, *J* = 7.6, 4.9 Hz, 2H), 7.31 (dd, *J* = 15.3, 7.6 Hz, 2H), 4.82 (d, *J* = 12.0 Hz, 1H), 4.70 (d, *J* = 12.1 Hz, 1H), 4.64 (s, 2H), 3.81 (q, *J* = 5.1 Hz, 1H), 3.68–3.31 (m, 82H), 2.15–2.06 (m, 3H). <sup>13</sup>C NMR (126 MHz, CDCl<sub>3</sub>) δ 141.57, 140.78, 140.71, 140.69, 140.63, 140.25, 140.23, 140.18, 140.13, 139.32, 138.87, 138.12, 138.06, 134.16, 132.06, 129.45, 128.94, 128.89, 128.07, 127.74, 127.70, 127.60, 127.32, 127.13, 126.92, 126.72, 126.66, 126.25, 126.08, 125.62, 125.32, 125.25, 124.92, 124.89, 77.54, 73.89, 72.42, 71.90, 71.60, 70.57, 70.53, 70.47, 70.42, 70.06, 70.00, 69.67, 69.48, 59.01, 40.25, 40.09. MALDI-TOF mass: *m/z* calcd. for C<sub>91</sub>H<sub>120</sub>NaO<sub>21</sub> [M + Na]<sup>+</sup>, 1572.930; found, 1571.307.

## Supporting Information

Supporting Information is available from the Wiley Online Library or from the author.

## Acknowledgements

This work was supported by the National Natural Science Foundation of China (21634005 and 51473062) and Fudan research fund.

## Conflict of Interest

The authors declare no conflict of interest.

## Keywords

helical tubules, self-assembly, stacked toroids, supramolecular polymerization

Received: March 14, 2020

Revised: April 5, 2020

Published online:

- [1] J. D. Mougous, M. E. Cuff, S. Ranuser, A. Shen, M. Zhou, C. A. Gifford, A. L. Goodman, G. Joachimiak, C. L. Ordoñez, S. Lory, T. Walz, A. Joachimiak, J. J. Mekalanos, *Science* **2006**, 312, 1526.
- [2] N. A. Yewdall, T. M. Allison, F. G. Pearce, C. V. Robinson, J. A. Gerrard, *Chem. Sci.* **2018**, 9, 6099.
- [3] F. Angelucci, A. Bellelli, M. Ardini, R. Ippoliti, F. Saccoccia, V. Morea, *FEBS J.* **2015**, 282, 2827.
- [4] N. A. Yewdall, H. Venugopal, A. Desfosses, V. Abrishami, Y. Yosaatmadja, M. B. Hampton, J. A. Gerrard, D. C. Goldstone, A. K. Mitra, M. Radjainia, *Structure* **2016**, 24, 1120.

- [5] S. Manuguri, K. Webster, N. A. Yewdall, Y. An, H. Venugopal, V. Bhugra, A. Turner, L. J. Domigan, J. A. Gerrard, D. E. Williams, J. Malmström, *Nano Lett.* **2018**, *18*, 5138.
- [6] B. Adhikari, Y. Yamada, M. Yamauchi, K. Wakita, X. Lin, K. Aratsu, T. Ohba, T. Karatsu, M. J. Hollamby, N. Shimizu, H. Takagi, R. Haruki, S. Adachi, S. Yagai, *Nat. Commun.* **2017**, *8*, 15254.
- [7] H.-J. Kim, Y.-B. Lim, M. Lee, *J. Polym. Sci., Part A: Polym. Chem.* **2008**, *46*, 1925.
- [8] Y. Kim, W. Li, S. Shin, M. Lee, *Acc. Chem. Res.* **2013**, *46*, 2888.
- [9] Z. Huang, S.-K. Kang, M. Banno, T. Yamaguchi, D. Lee, C. Seok, E. Yashima, M. Lee, *Science* **2012**, *337*, 1521.
- [10] H.-J. Kim, S.-K. Kang, Y.-K. Lee, C. Seok, J.-K. Lee, W.-C. Zin, M. Lee, *Angew. Chem., Int. Ed.* **2010**, *49*, 8471.
- [11] E. Lee, J.-K. Kim, M. Lee, *J. Am. Chem. Soc.* **2009**, *131*, 18242.
- [12] J. C. Nelson, J. G. Saven, J. S. Moore, P. G. Wolynes, *Science* **1997**, *277*, 1793.
- [13] Z. Huang, Y. Kim, T. Kim, M. Lee, *Polym. Chem.* **2013**, *4*, 268.
- [14] M. L. Bochman, A. Schwacha, *Microbiol. Mol. Biol. Rev.* **2009**, *73*, 652.
- [15] J. J. Lindeboom, M. Nakamura, A. Hibbel, K. Shundyak, R. Gutierrez, T. Ketelaar, A. M. C. Emons, B. M. Mulder, V. Kirik, D. W. Ehrhardt, *Science* **2013**, *342*, 1245533.
- [16] E. Zehr, A. Szyk, G. Piszczek, E. Szczesna, X. Zuo, A. Roll-Mecak, *Nat. Struct. Mol. Biol.* **2017**, *24*, 717.
- [17] J. M. Kollman, C. H. Greenberg, S. Li, M. Moritz, A. Zelter, K. K. Fong, J.-J. Fernandez, A. Sali, J. Kilmartin, T. N. Davis, D. A. Agard, *Nat. Struct. Mol. Biol.* **2015**, *22*, 132.
- [18] A. Klug, *Angew. Chem., Int. Ed. Engl.* **1983**, *22*, 565.
- [19] Y. Kim, H. Li, Y. He, X. Chen, X. Ma, M. Lee, *Nat. Nanotechnol.* **2017**, *12*, 551.
- [20] S. Yagai, M. Yamauchi, A. Kobayashi, T. Karatsu, A. Kitamura, T. Ohba, Y. Kikkawa, *J. Am. Chem. Soc.* **2012**, *134*, 18205.
- [21] M. Yamauchi, T. Ohba, T. Karatsu, S. Yagai, *Nat. Commun.* **2015**, *6*, 8936.
- [22] a) B. Shen, Y. Zhu, Y. Kim, X. Zhou, H. Sun, Z. Lu, M. Lee, *Nat. Commun.* **2019**, *10*, 1080; b) B. Shen, M. Lee, *Polym. Chem.* **2019**, *10*, 6551.
- [23] B. Shen, Y. He, Y. Kim, Y. Wang, M. Lee, *Angew. Chem., Int. Ed.* **2016**, *55*, 2382.
- [24] X. Liu, H. Li, Y. Kim, M. Lee, *Chem. Commun.* **2018**, *54*, 3102.
- [25] Z. Haung, H. Lee, S.-K. Kang, J.-M. Nam, M. Lee, *Nat. Commun.* **2011**, *2*, 459.
- [26] J. T. Chen, E. L. Thomas, C. K. Ober, G.-P. Mao, *Science* **1996**, *273*, 343.